

Signature of Nonadiabatic Coupling in Excited-State Vibrational Modes

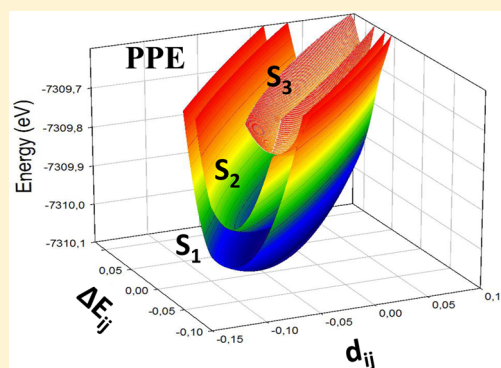
Miguel A. Soler,[†] Tammie Nelson,[‡] Adrian E. Roitberg,[§] Sergei Tretiak,^{*,‡}
and Sebastian Fernandez-Alberti^{*,†}

[†]Universidad Nacional de Quilmes, Roque Saenz Peña 352, B1876BXD Bernal, Argentina

[‡]Theoretical Division, Los Alamos National Laboratory, Los Alamos, New Mexico 87545, United States

[§]Quantum Theory Project, Department of Chemistry, University of Florida, Gainesville, Florida 32611, United States

ABSTRACT: Using analytical excited-state gradients, vibrational normal modes have been calculated at the minimum of the electronic excited-state potential energy surfaces for a set of extended conjugated molecules with different coupling between them. Molecular model systems composed of units of polyphenylene ethynylene (PPE), polyphenylenevinylene (PPV), and naphthacene/pentacene (NP) have been considered. In all cases except the NP model, the influence of the nonadiabatic coupling on the excited-state equilibrium normal modes is revealed as a unique highest frequency adiabatic vibrational mode that overlaps with the coupling vector. This feature is removed by using a locally diabatic representation in which the effect of NA interaction is removed. Comparison of the original adiabatic modes with a set of vibrational modes computed in the locally diabatic representation demonstrates that the effect of nonadiabaticity is confined to only a few modes. This suggests that the nonadiabatic character of a molecular system may be detected spectroscopically by identifying these unique state-specific high frequency vibrational modes.



INTRODUCTION

The photoinduced electronic and vibrational energy redistribution and relaxation in extended conjugated molecules plays an important role in chemical physics,¹ biology,² and materials science.³ Following photoexcitation, nonradiative transitions involving internal conversion, and intersystem crossing can occur.^{4,5} The photoinduced dynamics of extended conjugated molecules is often characterized by large nonadiabatic (NA) couplings between excited states.^{6,7} Therefore, it is crucial to discover the state-specific nuclear motions that promote energy funneling to the lowest excited state thus reinforcing the celebrated Kasha's rule,⁸ which is driven by NA couplings. Understanding the fundamental relationship between vibrational motions and the efficiency of NA nonradiative relaxation offers new routes toward materials-by-design approach for various applications and technologies.

Equilibrium normal modes (ENMs), typically calculated from second derivatives of the ground-state (GS) energy with respect to nuclear coordinates, can be used to identify relevant vibrational motions of polyatomic molecules.⁹ The simulation of complex processes involving many coupled electronic excited states requires state-specific normal modes defined according to the potential energy surfaces (PESs) involved. For this purpose, excited-state equilibrium normal modes (ES-ENMs) can be obtained using the excited-state PES. ES-ENMs are convenient for characterizing conical intersections,¹⁰ and they represent a straightforward way of examining experimental vibronic spectra by providing a decoupled description of vibrational motions.

Time-resolved observations of phonon dynamics, via fluorescence or transient absorption in the UV/vis and mid-IR spectral range, provide information on the excited-state dynamics of a molecule.¹¹ In this way, vibrational and structural information on chromophores can be directly measured. Vibrational bands are commonly assigned in terms of GS equilibrium normal modes (ENM(S_0)).¹² However, internal conversion often results from passage through several conical intersections and/or crossings between either interacting¹³ or noninteracting states.¹⁴ These passages may introduce a reordering and/or transient mixing, which changes the adiabatic state identities and causes modes to become mixed in regions of strong NA coupling. As a consequence, the normal mode identities of polyatomic molecules are generally not preserved upon electronic excitation.¹⁵ This Duschinsky effect introduces difficulties in calculating Franck–Condon factors,^{16,17} is responsible for relative changes in absorption and emission spectra,^{18,19} and can also affect Raman excitation profiles.²⁰ Gambetta and co-workers recently studied the relationship between ground and excited-state vibrations in single-walled carbon nanotubes using ultrashort visible pulses to generate and detect coherent phonons. Following photoexcitation,

Special Issue: Current Topics in Photochemistry

Received: April 4, 2014

Revised: May 16, 2014

Published: May 20, 2014

signatures of mode coupling were detected where the anharmonic coupling of excited-state vibrational wavepackets appeared as a frequency modulation in one of the modes.²⁰

In this article, we present an approach to characterize state-specific vibrations responsible for the intramolecular vibrational energy flow during nonradiative relaxation and identify their spectroscopic signature. It has recently been shown that the highest frequency *instantaneous* normal mode of the upper energy state significantly matches the corresponding NA coupling vector during NA transitions.²¹ However, instantaneous normal modes represent instant vibrational coordinates through which the nonequilibrium molecular dynamics can be analyzed but cannot be interpreted as real harmonic motion. Instead, excited-state *equilibrium* normal mode (ES-ENM) analysis at the local minimum of the corresponding excited-state PES is required.

The ES-ENM analysis is presented in terms of their participation in NA energy transfer between the chromophore units of a set of extended conjugated molecules. The magnitude of the NA coupling vector, defined as $\mathbf{d}_{\alpha\beta} = \langle \phi_{\alpha}(\mathbf{R}) | \nabla_{\mathbf{R}} \phi_{\beta}(\mathbf{R}) \rangle$ (where ϕ_{α} and ϕ_{β} are adiabatic excited-state wave functions and \mathbf{R} represents the nuclear coordinates), serves as a criterion for nonadiabaticity, and its direction corresponds to the direction of vibronic energy transfer during interstate NA transitions.²² In regions of strong coupling, the contribution to the forces in the direction of the NA coupling vector (Pechukas force²³) is the dominant factor for nuclear motion²⁴ and should be reflected in the specific adiabatic ES-ENMs responsible for the coupling. Furthermore, systems with a smaller displacement between the local excited-state PES minimum to a conical intersection seam (see Figure 1A) should exhibit stronger mode mixing and NA signatures in their ES-ENMs. Specifically, the projection of $\mathbf{d}_{\alpha\beta}$ on the basis of ES-ENMs with a significant agreement between $\mathbf{d}_{\alpha\beta}$ and a single mode indicates an effective decoupled nuclear direction for NA energy transfer to the specific vibrational degree of freedom.

Our aim is to characterize the electronic excited-state specific vibrations for a set of model systems. Such a framework is encouraging, as it can be validated through the development of new transient IR and ultrafast electronic spectroscopic studies focused on the intramolecular vibrational energy flow that takes place during the electronic excited-state relaxation. Spectroscopic detection of these modes would serve as a direct indication of NA interactions in molecular systems. Although this type of experiment is yet to be performed, excited-state IR spectroscopy,^{25–27} ultrafast time-resolved IR spectroscopy,^{28–30} and ultrafast transient IR spectroscopy³¹ have been shown to be powerful tools to study the decay of excited states.

MODELS AND METHODS

Model Systems. We perform ES-ENM analysis on the model systems shown in Figure 1B spanning a wide range of NA couplings and energy-level spacing. First, meta-linked linear polyphenylene ethynylene (PPE) units composed of 2-, 3-, and 4-rings represent building blocks for dendritic macromolecules.^{32,33} These fragments act as individual chromophores that localize excitons.^{34,35} The higher energy S_3 state is localized in the 2-ring unit, the S_2 state is localized in the 3-ring unit, and the lowest S_1 state is localized in the 4-ring unit.³⁴ As a result, photoinduced unidirectional energy transfer occurs in the 2-ring \rightarrow 3-ring \rightarrow 4-ring direction.³⁵ Next, 3- and 4-ring polyphenylenevinylene (PPV) oligomers are linked by a short or long alkyl chain (PPV- C_1 and PPV- C_{11} , respectively). PPV is

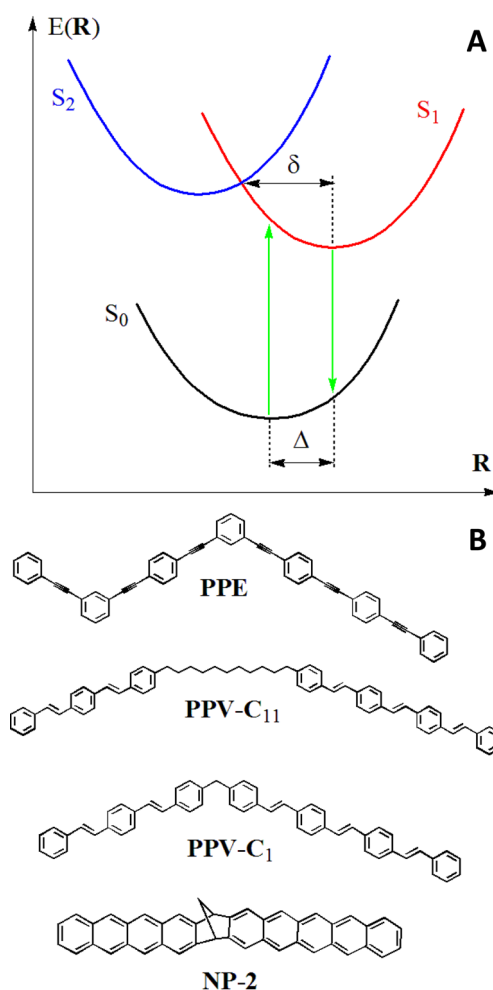


Figure 1. (A) Schematic of molecular potential energy surfaces as a function of vibrational coordinates showing the Franck–Condon displacement, Δ , and the displacement between the S_1 minimum and a nearby excited-state conical intersection, δ . (B) Chemical structures of model systems used for ES-ENM analysis.

a promising organic conjugated polymer for use in optoelectronic devices.³⁶ Torsional distortion of the PPV backbone can form conformational subfragments,^{37,38} and neighboring fragments can electronically couple to one another forming delocalized collective states that influence optical properties.³⁹ The absorption of each chromophore is not well separated giving rise to multiple energy transfer pathways.³⁷ Finally, a naphthacene-bridge-pentacene (NP-2) molecule is considered.⁴⁰ The naphthacene and pentacene are held at fixed distances and orientations by a rigid polynorbornyl-type bridge of two σ -bonds such that no molecular disorder due to torsional distortions is expected.

Excited-State Computational Methods. All excited-state calculations are performed at the configuration interaction singles (CIS) level using the Collective Electronic Oscillator (CEO) code⁴¹ combined with the Austin model 1 (AM1) semiempirical Hamiltonian.⁴² This methodology has previously been shown to provide an adequate description for excitonic states, interstate crossings, and NA dynamics in this class of molecular systems.^{34,37,43,44} Excited-state energies, gradients, and nonadiabatic coupling terms are computed analytically.^{45–49} This provides a convenient method for analyzing

the state-specific vibrations that participate in radiationless processes.

Excited-State Equilibrium Normal Mode Calculations. ES-ENMs are computed at the S_α state minimum from the mass-weighted Hessian matrix \mathbf{H}_α . The mass-weighted Cartesian *space-fixed* coordinates for the optimized configuration \mathbf{R}_0 are first translated and rotated to a *body-fixed* reference frame with the origin at the center of mass and axes corresponding to the principle axes of inertia. Within the Cartesian frame, the potential energy E_α for N nuclei moving on the α th electronic state is expanded to second order as

$$E_\alpha(\mathbf{R}) = \frac{1}{2} \sum_{i=1}^{3N} \sum_{j=1}^{3N} H_\alpha^{ij}(\mathbf{R}_0) \Delta R_i^i \Delta R_j^j \quad (1)$$

where $\Delta R_i^i = \mathbf{R}_i^i - \mathbf{R}_0^i$ is the displacement of atom $i = 1, \dots, N$ from its optimized configuration \mathbf{R}_0^i . Elements of the $3N$ -force vector \mathbf{F}_α are defined as $F_\alpha^i(\mathbf{R}_0) = -\partial E_\alpha / \partial R_i^i|_{\mathbf{R}_0}$, allowing $H_\alpha^{ij}(\mathbf{R}_0)$, with elements $H_\alpha^{ij}(\mathbf{R}_0) = -\partial E_\alpha / \partial R_i^i \partial R_j^j|_{\mathbf{R}_0}$ evaluated at the optimized configuration, \mathbf{R}_0 , to be computed numerically from finite differences of the gradients.

$$H_\alpha^{ii}(\mathbf{R}_0) = \frac{\partial^2 E_\alpha}{\partial R_i^i{}^2} = - \left[\frac{\frac{\partial F_\alpha^i(\mathbf{R}_0 + \delta R^i)}{\partial R^i} - \frac{\partial F_\alpha^i(\mathbf{R}_0 - \delta R^i)}{\partial R^i}}{2\delta R^i} \right] \quad (2)$$

and

$$H_\alpha^{ij}(\mathbf{R}_0) = \frac{1}{2} \left[\frac{\partial^2 E_\alpha}{\partial R_i^i \partial R_j^j} + \frac{\partial^2 E_\alpha}{\partial R_j^j \partial R_i^i} \right] \quad (3)$$

$$H_\alpha^{ij}(\mathbf{R}_0) = - \left[\frac{\frac{\partial F_\alpha^i(\mathbf{R}_0 + \delta R^j)}{\partial R^j} - \frac{\partial F_\alpha^i(\mathbf{R}_0 - \delta R^j)}{\partial R^j}}{2\delta R^j} \right] - \left[\frac{\frac{\partial F_\alpha^j(\mathbf{R}_0 + \delta R^i)}{\partial R^i} - \frac{\partial F_\alpha^j(\mathbf{R}_0 - \delta R^i)}{\partial R^i}}{2\delta R^i} \right] \quad (4)$$

where δR^i is a finite displacement of the coordinate R^i .

Diagonalization of \mathbf{H}_α produces a set of orthonormal ES-ENM(S_α) with frequencies ν_α^i related to the eigenvalues λ_α^i ($i = 1, \dots, 3N - 6$) of \mathbf{H}_α as $\nu_\alpha^i = ((\lambda_\alpha^i)^{1/2})/2\pi$. The ES-ENM vectors $\{\mathbf{Q}_\alpha^i\}_{i=1, 3N-6}$ can be expressed as a linear combination of Cartesian displacements

$$\mathbf{Q}_\alpha^i = \sum_{j=1}^{3N-6} l_\alpha^{ij} \Delta \mathbf{R}_j^j \quad (5)$$

where l_α^{ij} are elements of the eigenvector matrix \mathbf{L}_α .

Some numerical sensitivity in the frequency of \mathbf{Q}_α^{3N-6} to the value of δR^i was observed. This is expected due to the sharp peaks in the NA couplings particularly in cases where the S_α minimum is close to an unavoided crossing with $S_{\alpha-1}$. However, the shape of the corresponding normal mode eigenvectors is not sensitive to the coordinate displacement.

Locally Diabatic Representation. We use the locally diabatic representation developed by Granucci and Persico⁵⁰ in order to remove the effect of nonadiabatic interaction on the excited state electronic wave function along the considered nuclear displacement. First, the overlap matrix $\mathbf{S}(\mathbf{R}_0; \mathbf{R}_0 \pm \delta R^i)$ with elements

$$S_{\alpha\beta}(\mathbf{R}_0; \mathbf{R}_0 \pm \delta R^i) = \phi_\alpha(\mathbf{r}; \mathbf{R}_0) \cdot \phi_\beta(\mathbf{r}; \mathbf{R}_0 \pm \delta R^i) \quad (6)$$

is evaluated where \mathbf{r} represents the electronic coordinates and $\phi_\alpha(\mathbf{r}; \mathbf{R}_0)$ and $\phi_\beta(\mathbf{r}; \mathbf{R}_0 \pm \delta R^i)$ are the CIS excited state adiabatic wave functions evaluated at equilibrium and displaced configurations, respectively. The unitary transformation \mathbf{T} connecting the adiabatic and diabatic representations for each specific displacement $\pm \delta R^i$ is approximated by Löwdin's orthogonalization

$$\mathbf{T} = \mathbf{S}(\mathbf{R}_0; \mathbf{R}_0 \pm \delta R^i) \mathbf{O} \Lambda^{-1/2} \mathbf{O}^t \quad (7)$$

where Λ is the diagonal eigenvalue matrix of $\mathbf{S}(\mathbf{R}_0; \mathbf{R}_0 \pm \delta R^i) \mathbf{S}(\mathbf{R}_0; \mathbf{R}_0 \pm \delta R^i)$ and \mathbf{O} is the diagonalizing transformation

$$\mathbf{S}(\mathbf{R}_0; \mathbf{R}_0 \pm \delta R^i) \mathbf{S}(\mathbf{R}_0; \mathbf{R}_0 \pm \delta R^i) \mathbf{O} = \mathbf{O} \Lambda \quad (8)$$

Applying \mathbf{T} as

$${}^D\mathbf{F}_{\alpha\beta}^i(\mathbf{R}_0 \pm \delta R^i) = \mathbf{T} \mathbf{F}_{\alpha\beta}^i(\mathbf{R}_0 \pm \delta R^i) \mathbf{T}^t \quad (9)$$

where the adiabatic force matrix computed at $\mathbf{R}_0 \pm \delta R^i$ is given by

$$\mathbf{F}_{\alpha\beta}^i(\mathbf{R}_0 \pm \delta R^i) = \begin{pmatrix} F_{\alpha\alpha}^i(\mathbf{R}_0 \pm \delta R^i) & 0 \\ 0 & F_{\beta\beta}^i(\mathbf{R}_0 \pm \delta R^i) \end{pmatrix} \quad (10)$$

results in the following diabatic force matrix

$${}^D\mathbf{F}_{\alpha\beta}^i(\mathbf{R}_0 \pm \delta R^i) = \begin{pmatrix} {}^D F_{\alpha\alpha}^i(\mathbf{R}_0 \pm \delta R^i) & {}^D F_{\alpha\beta}^i(\mathbf{R}_0 \pm \delta R^i) \\ {}^D F_{\beta\alpha}^i(\mathbf{R}_0 \pm \delta R^i) & {}^D F_{\beta\beta}^i(\mathbf{R}_0 \pm \delta R^i) \end{pmatrix} \quad (11)$$

whose diagonal elements ${}^D F_{\alpha\alpha/\beta\beta}^i(\mathbf{R}_0 \pm \delta R^i)$ represent forces associated with diabatic electronic states whose identities do not change during coordinate displacement. Neglecting cross terms, we construct a set of locally diabatic ES- D ENM (in the following, the superscript D denotes quantities in the locally diabatic representation) represented by vectors $\{{}^D\mathbf{Q}_\alpha^i\}_{i=1, 3N-6}$ and frequencies ${}^D\nu_\alpha^i$ ($i = 1, \dots, 3N - 6$) where NA interaction is removed.

Transition Density Localization. Excited vibrational modes should involve the motion of the nuclei where the excitation is localized. This can be determined from the spatial localization of the electronic transition density (TD). Transition density matrices $(\rho^{0\alpha})_{nm} \equiv \langle \phi_\alpha(t) | c_n^+ c_m | \phi_0(t) \rangle$ are computed using the CEO approach⁵¹ where c_n^+ (c_m) are creation (annihilation) operators, n and m denote atomic orbital (AO) basis functions, and $\phi_0(t)$ and $\phi_\alpha(t)$ are the CIS adiabatic wave functions for the ground and excited state, respectively. Therefore, the diagonal elements $(\rho^{0\alpha})_{nn}$ represent the net change in the electronic density induced on an atomic orbital for a ground to excited state electronic transition. The total electronic transition density can be found by summing the contributions of the atomic orbitals of each atom in the molecule.

RESULTS

Characterization of PES Minima. For configurations where the interaction between electronic states becomes relevant, interchromophore energy transfer takes place and vibrational motions get excited in the direction of the NA coupling vector $\mathbf{d}_{\alpha(\alpha-1)}$. As shown in Figure 2, $\mathbf{d}_{\alpha(\alpha-1)}$ evaluated

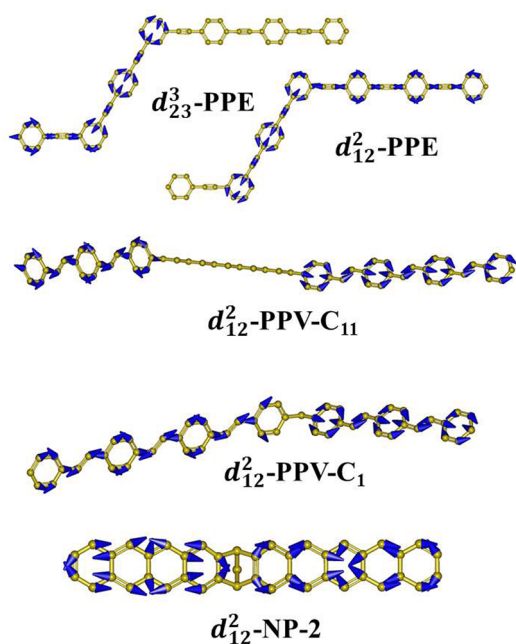


Figure 2. NA coupling vectors between S_α and $S_{\alpha-1}$ at the S_α PES minimum.

at the minimum of the S_α PES (in our notation, the superindex α indicates the electronic state of the minimum at which a variable is evaluated), involves significant nuclear displacements on both fragments consistent with their roles as pathways through which efficient energy funneling occurs.^{21,35} Only the major contribution to $\mathbf{d}_{\alpha(\alpha-1)}^\alpha$ composed of C–C stretches are shown in Figure 2 for clarity. The magnitude of $\mathbf{d}_{\alpha(\alpha-1)}^\alpha$ (see Table 1) is largest for PPV and PPE systems and much smaller in the rigid NP-2 system.

The strength of the NA interaction, $|\mathbf{d}_{\alpha(\alpha-1)}^\alpha|$, at the S_2 minimum in PPV- C_{11} compared to PPV- C_1 is not unexpected. The close proximity of the chromophores in PPV- C_1 leads to large excitonic coupling (should be distinguished from the NA coupling $\mathbf{d}_{\alpha(\alpha-1)}^\alpha$) caused by electrostatic interactions between state TDs.^{41,44} Therefore, the appearance of a large Davydov splitting between S_α and $S_{\alpha-1}$ in PPV- C_1 lessens the effective NA coupling compared to that of PPV- C_{11} . Overall, in all cases, except NP-2, where molecular rigidity prevents distortions, there is a strong NA interaction between S_α and $S_{\alpha-1}$ at the S_α PES minimum. This large value of $|\mathbf{d}_{\alpha(\alpha-1)}^\alpha|$ along with excitonic

coupling induces wave function mixing and delocalization between chromophore units. In order to analyze that, electronic TDs, $\rho^{0\alpha}$ and $\rho^{0(\alpha-1)}$, evaluated at the S_α minimum are shown in Figure 3. In all cases except NP-2, S_α and $S_{\alpha-1}$ TDs are

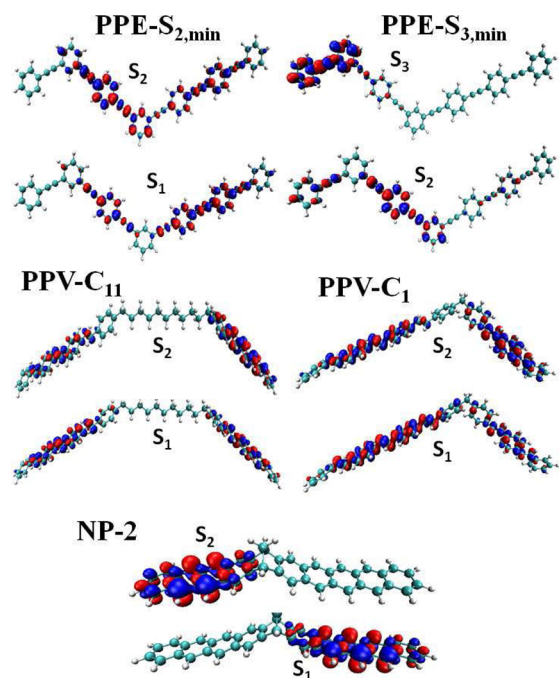


Figure 3. Electronic transition densities for states S_α and $S_{\alpha-1}$ at the S_α PES minimum.

delocalized. In the absence of significant interactions, S_α and $S_{\alpha-1}$ should be localized as seen for NP-2. Careful comparison of Figures 2 and 3 reveals that the vibrational motions involve the displacement of nuclei where the electronic transition density is localized.

Nonadiabatic events are usually represented in terms of the space spanned by the coordinates along the energy difference gradient, $\partial(E_\alpha - E_{\alpha-1})/\partial\mathbf{R}$, and NA coupling $\mathbf{d}_{\alpha(\alpha-1)}^\alpha$ vectors.^{52,53} This provides a branching space^{54,55} in which the degeneracy of conical intersections is lifted. In Figure 4A, the optimized S_α geometry is positioned at the origin, and the S_α and $S_{\alpha-1}$ surfaces are plotted in the branching space where $\mathbf{R} = \mathbf{R}_0 + \mathbf{g}\mathbf{d}_{\alpha(\alpha-1)}^\alpha + \mathbf{h}\partial(E_\alpha - E_{\alpha-1})/\partial\mathbf{R}$. Starting at the equilibrium geometry \mathbf{R}_0 , the structure is distorted in the direction of either

Table 1. NA Coupling Strengths and ES-ENM Analysis in Model Systems

	PPE (S_3)	PPE (S_2)	PPV- C_{11} (S_2)	PPV- C_1 (S_2)	NP-2 (S_2)
$ \mathbf{d}_{\alpha(\alpha-1)}^\alpha $ (au)	9.9	13.6	73	10.4	3.5
$\Delta E_{\alpha(\alpha-1)}^\alpha$ (eV)	0.06	0.12	0.01	0.10	0.05
$ \mathbf{d}_{\alpha(\alpha-1)}^{\alpha-1} $ (au)	1.7	0.9	0.1	0.8	0.7
a_α^{\max} (mode)	0.9 (246)	0.9 (246)	0.9 (369)	0.7 (279)	0.9 (175)
$D_{a_\alpha^{\max}}$ (mode)	0.8 (216)	0.9 (216)	0.8 (307)	0.8 (238)	0.9 (175)
$\nu(D_{a_\alpha^{\max}})$ (cm^{-1})	3121.4	3011.1	2859.4	3050.4	2678.2
$D\mathbf{P}_{\mathbf{d}_{\alpha(\alpha-1)}^\alpha}^D$	1.6	1.3	1.7	1.5	1.1
$D\mathbf{P}_{\mathbf{d}_{\alpha(\alpha-1)}^{\alpha-1}}^D$	7.4	6.2	12	18.8	1.8
% modes $ \Delta\nu < 5 \text{ cm}^{-1}$	96	97	93	98	99
% modes $ \langle \mathbf{D}\mathbf{Q}_i^\alpha, \mathbf{Q}_i^{\alpha-1} \rangle > 0.9$	87	90	61	91	96
$D\mathbf{P}_{\mathbf{D}\mathbf{Q}_i^{\max}}^D$	4.3	3.4	8.6	8.3	4.4
$\langle \mathbf{D}\mathbf{Q}_i^\alpha, \mathbf{Q}_i^{\alpha-1} \rangle$	0.8	0.8	0.7	0.7	0.9

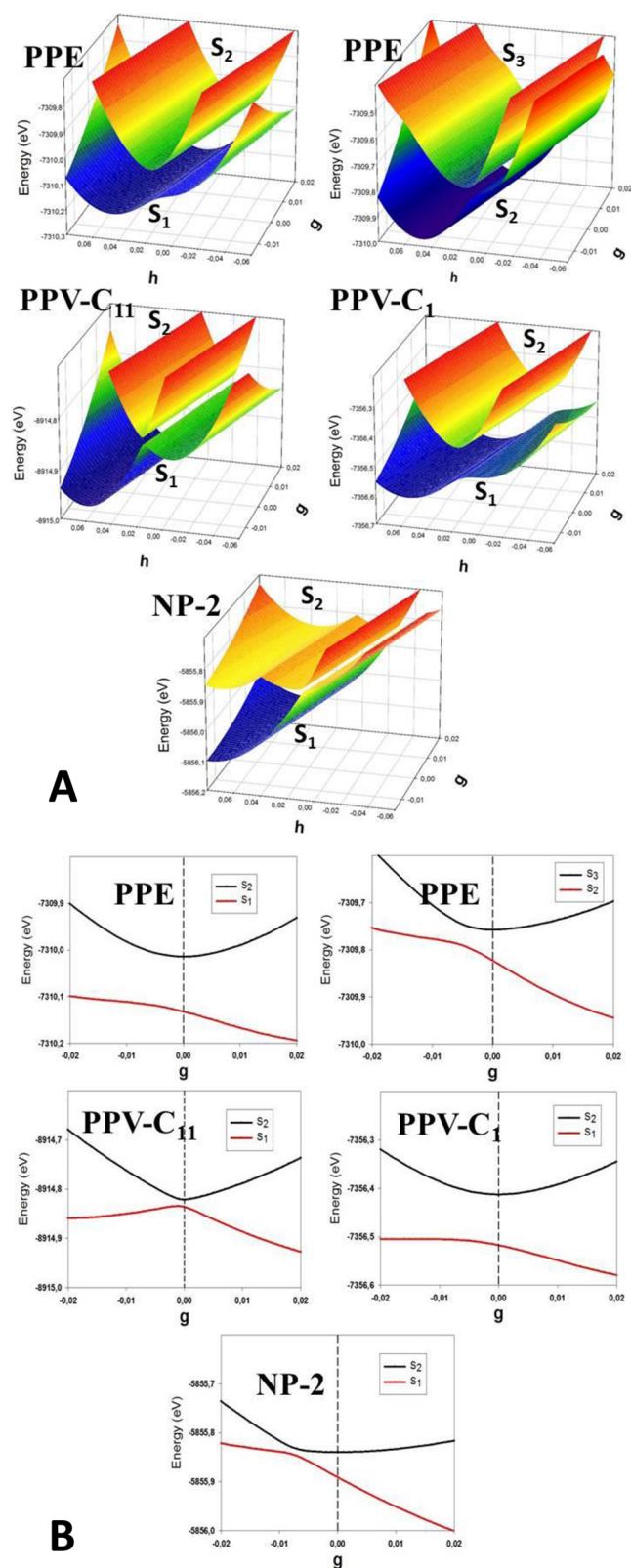


Figure 4. (A) Potential energy surfaces for states S_α and $S_{\alpha-1}$ in the branching space spanned by the gradient difference (h) and the NA coupling vectors (h) around the minimum of S_α positioned at the origin. (B) Variation of the potential energy for S_α and $S_{\alpha-1}$ as a function of the NA coupling vector (g) for $h = 0$. Energy gaps are defined at the S_α minimum appearing at the origin.

the NA coupling vector (g) or in the direction of the energy difference gradient (h). These two vectors are normalized, and their directions remain fixed to the ones at the minimum.

As can be seen in Figure 4A, the minima of the S_α surfaces are commonly in regions of the branching space with relatively small energy gaps with the $S_{\alpha-1}$ surfaces. According to the Hellmann–Feynman theorem, the nonadiabatic coupling scales as $1/\Delta E$. Therefore, the S_α equilibrium geometries are potentially influenced by strong NA couplings between states. The energy gap, $\Delta E_{\alpha(\alpha-1)}^\alpha$, between S_α and $S_{\alpha-1}$ surfaces at the S_α minimum can be seen in Figure 4B where the variation of the potential energy of S_α and $S_{\alpha-1}$ is plotted in the direction of the NA coupling vector with the optimized S_α geometry positioned at the origin. These plots represent slices of the surfaces in Figure 4A along the g axis with $h = 0$. The energy gap, $\Delta E_{\alpha(\alpha-1)}^\alpha$, varies among the models (see Table 1), being the smallest for PPV-C₁₁. While the small energy gap for PPV-C₁₁ can be associated with the larger NA coupling $|d_{21}^2|$ between units, there is no clear relationship between the magnitude of the NA coupling $|d_{\alpha(\alpha-1)}^\alpha|$ and the energy gap $\Delta E_{\alpha(\alpha-1)}^\alpha$ for the other systems. The surfaces for PPE, PPV-C₁₁, PPV-C₁, and NP-2 in Figure 4A can be misinterpreted as having no dependence on $d_{\alpha(\alpha-1)}^\alpha$ where the local minima appear to be parallel to the g axis. The g dependence can be seen more clearly from Figure 4B. As we have previously stressed, the direction of $d_{\alpha(\alpha-1)}^\alpha$ has an important physical meaning²¹ since it represents the nonadiabatic contribution to the nuclear forces. Therefore, structural distortions in the direction of $d_{\alpha(\alpha-1)}^\alpha$ can be interpreted as displacements in the direction of effective vibronic energy transfer throughout regions of strong NA coupling.

ES-ENM Analysis. Agreement between $d_{\alpha\beta}$ and a single mode indicates an effective decoupled nuclear direction for NA energy transfer. To investigate this, the NA coupling vector $d_{\alpha(\alpha-1)}^\alpha$ is projected on the basis set of the ES-ENM(S_α) as

$$d_{\alpha(\alpha-1)}^\alpha = \sum_{j=1}^{3N-6} a_\alpha^j \mathbf{Q}_\alpha^j \quad (12)$$

It is remarkable that in all cases, except NP-2, the maximum value a_α^{\max} corresponds to the highest frequency ES-ENM(S_α) such that $d_{\alpha(\alpha-1)}^\alpha \approx \mathbf{Q}_\alpha^{3N-6}$. Such high frequencies result from a large magnitude of the NA coupling vector, which changes rapidly in the direction of the crossing seam and leads to mode mixing. These modes represent convolutions of high frequency motions. The resulting displacements are sensitive to the particular form of $d_{\alpha(\alpha-1)}^\alpha$ and involve atoms participating in $d_{\alpha(\alpha-1)}^\alpha$ where the electron density is localized (Figures 2 and 3). The major contributions are primarily composed of in-plane benzene ring C–C stretches (NP-2) with the addition of C–C stretching in the direction of the ethynylene (PPE) or vinylene (PPV) bonds (see Figure 2) combined with minor contributions from the high frequency collective C–H stretching.

Next, we make use of the locally diabatic representation. The projection of $d_{\alpha(\alpha-1)}^\alpha$ on the basis set of the ES-^DENM(S_α) as

$$d_{\alpha(\alpha-1)}^\alpha = \sum_{j=1}^{3N-6} d_\alpha^{jD} \mathbf{Q}_\alpha^j \quad (13)$$

results in a negligible overlap with the highest frequency normal mode. The maximum $d_\alpha^{D,\max}$ and corresponding $^D\mathbf{Q}_\alpha^{\max}$ mode number and frequency ν are given in Table 1. As expected, the ES-ENM of NP-2 are unaffected by the locally diabatic

representation due to the relatively small magnitude of the NA coupling $|\mathbf{d}_{\alpha(\alpha-1)}^\alpha|$ in that system. The participation number for the projections is given by

$${}^D\mathbf{P}_{\mathbf{d}_{\alpha(\alpha-1)}^\alpha}^\alpha = \left(\sum_{j=1}^{3N-6} ({}^D a_{\alpha}^j)^4 \right)^{-1} \quad (14)$$

This quantity represents the number of modes that contribute to the NA coupling vector. ${}^D\mathbf{P}_{\mathbf{d}_{\alpha(\alpha-1)}^\alpha}^\alpha \approx 3N - 6$ corresponds to the fully delocalized $\mathbf{d}_{\alpha(\alpha-1)}^\alpha$ with contributions from every ES- D ENM(S_α), whereas ${}^D\mathbf{P}_{\mathbf{d}_{\alpha(\alpha-1)}^\alpha}^\alpha \approx 1$ corresponds to $\mathbf{d}_{\alpha(\alpha-1)}^\alpha$ being identical to a unique ES- D ENM(S_α). As seen in Table 1, $\mathbf{d}_{\alpha(\alpha-1)}^\alpha$ is characterized by one or two ES- D ENM(S_α) meaning that there are at least two unique high frequency modes that represent the NA coupling in all cases considered.

The correspondence between adiabatic ES-ENMs and ES- D ENMs computed in a locally diabatic representation^{50,56} reveals the extent of mode mixing due to NA coupling. Both sets of modes have been compared using the Min-Cost algorithm⁵⁷ to assign the ES- D ENM(S_α) using the ES-ENM(S_α) as templates. The original adiabatic modes have a correspondence with their assigned diabatic modes where more than 90% of the modes have frequency variations $|\Delta\nu| < 5 \text{ cm}^{-1}$ (see Table 1). In addition, the overlap between each ES-ENM(S_α) and corresponding ES- D ENM(S_α), $|\langle \mathbf{Q}_\alpha^i, \mathbf{Q}_\alpha^j \rangle|$ (see Table 1), shows that about 90% of the modes have an overlap greater than 0.9 for all systems except PPV-C₁₁ indicating the relevant effect of the strong NA interaction (large $|\mathbf{d}_{\alpha(\alpha-1)}^\alpha|$ value) on the identity of state-specific vibrations for that system. The comparison between ES-ENM(S_α) and ES- D ENM(S_α) for PPE is shown in Figure 5. For both ES- D ENM(S_3) and

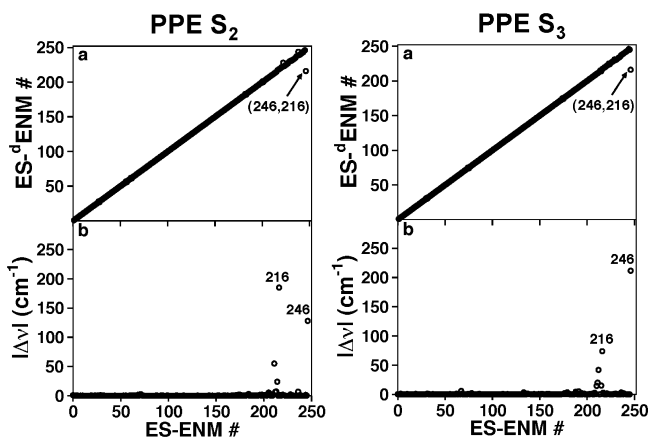


Figure 5. (a) Assignment and (b) variation in the frequency $|\Delta\nu|$ of the ES- D ENM with respect to ES-ENM calculated at the minimum of S_3 (right) and S_2 (left) for PPE.

ES- D ENM(S_2), the 246th and 216th modes have the most significant perturbation in their frequencies (corresponding to a_{α}^{\max} and d_{α}^{\max} modes). Smaller changes in modes 210–212 ES- D ENM(S_3) and 210–214 ES- D ENM(S_2) can be observed in Figure 5. Therefore, the effect of the nonadiabatic interaction between S_α and $S_{\alpha-1}$ is confined to only a few perturbed modes that are coupled to each other but decoupled from the other modes. Otherwise, both sets of ES-ENM are quite similar.

While the effect of NA interaction between S_α and $S_{\alpha-1}$ is generally confined to only a few modes at the S_α PES minimum, this is not true at the corresponding $S_{\alpha-1}$ minimum.

In that case, $|\mathbf{d}_{\alpha(\alpha-1)}^\alpha|$ is significantly smaller than $|\mathbf{d}_{\alpha(\alpha-1)}^\alpha|$ indicating that S_α and $S_{\alpha-1}$ are much less coupled at the $S_{\alpha-1}$ minimum. Furthermore, the participation number at the $S_{\alpha-1}$ minimum, ${}^D\mathbf{P}_{\mathbf{d}_{\alpha(\alpha-1)}^\alpha}^{\alpha-1}$ is large, and the NA coupling vector is spread among several modes (see Table 1).

The correspondence between ENM(S_0) and ES-ENM can be explored using a Duschinsky⁵⁸ linear transformation of the original ENM(S_0). The ES- D ENM(S_α) representing d_{α}^{\max} can be approximated by GS vibrational modes by projecting the ES- D ENM(S_α) on the basis of ENM(S_0) $\{\mathbf{Q}_0^i\}_{i=1 \dots 3N-6}$ calculated at the GS minimum as

$${}^D\mathbf{Q}_\alpha^{\max} = \sum_{j=1}^{3N-6} {}^D b_0^j {}^D \mathbf{Q}_0^j \quad (15)$$

The corresponding participation numbers

$${}^D\mathbf{P}_{{}^D\mathbf{Q}_\alpha^{\max}}^0 = \left(\sum_{j=1}^{3N-6} ({}^D b_0^j)^4 \right)^{-1} \quad (16)$$

reported in Table 1 reveal that multiple GS modes are involved rather than one or two distinct modes as in ${}^D\mathbf{P}_{\mathbf{d}_{\alpha(\alpha-1)}^\alpha}^\alpha$. The average overlap between each ES- D ENM(S_α) and its corresponding ENM(S_0), $|\langle {}^D\mathbf{Q}_\alpha^i, \mathbf{Q}_0^j \rangle|$, is also given in Table 1. Both sets of modes have a similarity greater than 70%, confirming that Duschinsky rotations are not large for most of the modes. Nevertheless, the lack of a GS decoupled vibration in the direction of ${}^D\mathbf{Q}_\alpha^{\max}$ highlights the weakness of simplifications, such as the classical path approximation,⁵⁹ to describe the NA process responsible for funneling energy to the lowest excited state.

CONCLUSIONS

ES-ENM analysis has been performed for a set of extended conjugated molecules composed of linked chromophore units with different coupling between them. Inclusion of NA interactions in the ES-ENM calculation leads to the highest frequency adiabatic normal mode that perfectly matches the NA coupling vector. The correspondence between adiabatic ES-ENM(S_α) and ES- D ENM(S_α) computed in a locally diabatic representation where the effect of NA interaction has been removed allows modes related to NA coupling to be easily identified. Both sets of modes are quite similar, with the exception of one or two high frequency modes related to the NA interaction. The efficient internal conversion that occurs during energy relaxation can be explained in terms of the differential participation of state-specific vibrations. The NA coupling at the “upper” S_α PES minimum is significantly strong, and unique modes contribute to the NA coupling vector indicating an effective direction for NA energy transfer decoupled from the other modes. However, NA coupling is much weaker at the “lower” $S_{\alpha-1}$ surface where the scattering of $\mathbf{d}_{\alpha\beta}$ within multiple ES-ENMs indicates reduced vibronic NA energy transfer efficiency. While Duschinsky rotations are not large for most of the modes, the ES- D ENM cannot always be assigned to equivalent GS modes. Therefore, a reduced set of state-specific vibrations is responsible for intramolecular energy transfer during nonradiative relaxation. In summary, our findings encourage the development of methods suited to preferentially treat the reduced subspace of state-specific vibrations responsible for intramolecular energy transfer during electronic relaxation. Future studies are needed to address

fundamental questions such as the effects of electronic or nuclear quantum coherence. Most significantly, the results suggest a distinct spectroscopic signature for NA interactions in molecular systems. The detection of these unique high frequency vibrational modes via time-resolved IR spectroscopies can be interpreted as evidence of NA effects. Furthermore, we propose that these modes may offer a route toward optical control by selectively driving these modes in order to promote the associated NA process.

AUTHOR INFORMATION

Corresponding Authors

*(S.T.) E-mail: serg@lanl.gov.

*(S.F.-A.) E-mail: sfalberti@gmail.com.

Notes

The authors declare no competing financial interest.

ACKNOWLEDGMENTS

This work was partially supported by CONICET, UNQ, ANPCyT (PICT-2010-2375), National Science Foundation Grant No. CHE-0239129 and CHE-0808910, and U.S. Department of Energy and Los Alamos LDRD funds. Los Alamos National Laboratory is operated by Los Alamos National Security, LLC, for the National Nuclear Security Administration of the U.S. Department of Energy under contract DE-AC5206NA25396. The authors acknowledge support from the Center for Integrated Nanotechnologies (CINT) and the Center for Nonlinear Studies (CNLS) at LANL.

REFERENCES

- (1) Olivucci, M. *Computational Photochemistry*; Elsevier: Amsterdam, The Netherlands, 2005.
- (2) Worth, G. A.; Cederbaum, L. S. Mediation of Ultrafast Electron Transfer in Biological Systems by Conical Intersections. *Chem. Phys. Lett.* **2001**, *338*, 219–223.
- (3) Lasorne, B.; Worth, G. A.; Robb, M. A. Excited-State Dynamics. *WIREs Comput. Mol. Sci.* **2011**, *1*, 460–475.
- (4) Olivucci, M.; Robb, M. A.; Bernardi, F. *Conformational Analysis of Molecules in Excited States*; Wiley-VCH: New York, 2000.
- (5) Yarkony, D. R. Nonadiabatic Quantum Chemistry: Past, Present, and Future. *Chem. Rev.* **2012**, *112*, 481–498.
- (6) Karabunarliev, S.; Baumgarten, M.; Bittner, E.; Mullen, K. Rigorous Franck-Condon Absorption and Emission Spectra of Conjugated Oligomers from Quantum Chemistry. *J. Chem. Phys.* **2000**, *113*, 11372.
- (7) Tretiak, S.; Saxena, A.; Martin, R. L.; Bishop, A. R. Conformational Dynamics of Photoexcited Conjugated Molecules. *Phys. Rev. Lett.* **2002**, *89*, 097402.
- (8) Kasha, M. Characterization of Electronic Transitions in Complex Molecules. *Discuss. Faraday Soc.* **1950**, *9*, 14–19.
- (9) Brooks, B.; Karplus, M.; Pettitt, B. M. Proteins: A Theoretical Perspective of Dynamics, Structure, and Thermodynamics. *Adv. Chem. Phys.* **1988**, *71*, 1–6.
- (10) Sicilia, F.; Blancafort, L.; Bearpark, M. J.; Robb, M. A. Quadratic Description of Conical Intersections: Characterization of Critical Points on the Extended Seam. *J. Phys. Chem. A* **2007**, *111*, 2182–2192.
- (11) Nibbering, E. T. J.; Fidler, H.; Pines, E. Ultrafast Chemistry: Using Time-Resolved Vibrational Spectroscopy for Interrogation of Structural Dynamics. *Annu. Rev. Phys. Chem.* **2005**, *56*, 337–367.
- (12) Kurtz, L.; Hofmann, A.; De Vivie-Riedle, R. Ground State Normal Mode Analysis: Linking Excited State Dynamics and Experimental Observables. *J. Chem. Phys.* **2001**, *114*, 6151–6159.
- (13) Worth, G. A.; Cederbaum, L. S. Beyond Born–Oppenheimer: Molecular Dynamics Through a Conical Intersection. *Annu. Rev. Phys. Chem.* **2004**, *55*, 127–158.
- (14) Fernandez-Alberti, S.; Roitberg, A. E.; Nelson, T.; Tretiak, S. Identification of Unavoided Crossings in Nonadiabatic Photoexcited Dynamics Involving Multiple Electronic States in Polyatomic Conjugated Molecules. *J. Chem. Phys.* **2012**, *137*, 014512.
- (15) Zgierski, M. Z. On Mode Mixing Effects in Absorption-Emission Spectra and Resonance Raman Excitation Profiles. *Chem. Phys.* **1986**, *108*, 61–68.
- (16) Doktorov, E. V.; Malkin, I. A.; Man'ko, V. I. The Dushinsky Effect and Sum Rules for Vibronic Transitions in Polyatomic Molecules. *J. Mol. Spectrosc.* **1979**, *77*, 178–194.
- (17) Reimers, J. R. A Practical Method for the use of Curvilinear Coordinates in Calculations of Normal-Mode-Projected Displacements and Duschinsky Rotation Matrices for Large Molecules. *J. Chem. Phys.* **2001**, *115*, 9103–9109.
- (18) Orr, G.; Small, C. J. Vibronic Intensity Borrowing and the Isotope Dependence of Vibronic Structure. *Chem. Phys.* **1973**, *2*, 60–68.
- (19) Metz, F.; Robey, M. J.; Schlag, E. W.; Dorr, F. Vibronic Coupling and the Duschinsky Effect in Benzene. *Chem. Phys. Lett.* **1977**, *51*, 8–12.
- (20) Gambetta, A.; Manzoni, C.; Menna, E.; Meneghetti, M.; Cerullo, G.; Lanzani, G.; Tretiak, S.; Piryatinski, A.; Saxena, A.; Martin, R. L.; et al. Real-Time Observation of Nonlinear Coherent Phonon Dynamics in Single-Walled Carbon Nanotubes. *Nat. Phys.* **2006**, *2*, 515–520.
- (21) Soler, M.; Roitberg, A. E.; Nelson, T.; Tretiak, S.; Fernandez-Alberti, S. Analysis of State-Specific Vibrations Coupled to the Unidirectional Energy Transfer in Conjugated Dendrimers. *J. Phys. Chem. A* **2012**, *116*, 9802–9810.
- (22) Tully, J. C. Nonadiabatic Molecular Dynamics. *Int. J. Quantum Chem.* **1991**, *40*, 299–309.
- (23) Pechukas, P. Time-Dependent Semiclassical Scattering Theory. II. Atomic Collisions. *Phys. Rev.* **1969**, *181*–185, 174.
- (24) Webster, F.; Schnitker, J.; Friedrichs, M. S.; Friesner, R. A.; Rossky, P. J. Solvation Dynamics of the Hydrated Electron: A Nonadiabatic Quantum Simulation. *Phys. Rev. Lett.* **1991**, *66*, 3172–3175.
- (25) Weiler, M.; Bartl, K.; Gerhards, M. Infrared/Ultraviolet Quadruple Resonance Spectroscopy to Investigate Structures of Electronically Excited States. *J. Chem. Phys.* **2012**, *136*, 114202.
- (26) Chen, Y.; Palmer, P. M.; Topp, M. R. Infrared Spectroscopy of Jet-cooled, Electronically Excited Clusters of Coumarin 151: Excited-State Interactions and Conformational Relaxation. *Int. J. Mass Spectrom.* **2002**, *220*, 231251.
- (27) Seurre, N.; Le Barbu-Debus, K.; Lahmani, F.; Zehnacker-Rentien, A.; Sepiol, J. Electronic and Vibrational Spectroscopy of Jet-Cooled Mcyanophenol and Its Dimer: Laser-Induced Fluorescence and Fluorescence-dip IR Spectra in the S₀ and S₁ States. *Chem. Phys.* **2003**, *295*, 2133.
- (28) Zhang, Y.; Burdzinski, G.; Kubicki, J.; Vyas, S.; Hadad, C. M.; Silwa, M.; Poizat, O.; Buntinx, G.; Platz, M. S. Study of the S₁ Excited State or *para*-Methoxy-3-phenyl-3-methyl Diazirine by Ultrafast Time Resolved UV-Vis and IR Spectroscopies and Theory. *J. Am. Chem. Soc.* **2009**, *131*, 13784.
- (29) Zhang, Y.; Kubicki, J.; Platz, M. S. Ultrafast UV-Visible and Infrared Spectroscopic Observation of a Singlet Vinylcarbene and the Intramolecular Cyclopropanation Reaction. *J. Am. Chem. Soc.* **2009**, *131*, 1360213603.
- (30) Vyas, S.; Kubicki, J.; Luk, H. L.; Zhang, Y.; Gritsan, N. P.; Hadad, C. M.; Platz, M. S. An Ultrafast Time-Resolved Infrared and UV-Vis Spectroscopic and Computational Study of the Photochemistry of AcylAzides. *J. Phys. Org. Chem.* **2012**, *25*, 693703.
- (31) Dougherty, T. P.; Heilweil, E. J. Ultrafast Transient Infrared Absorption Studies of M(CO)₆ (M = Cr, Mo or W) Photoproducts in *n*-Hexane Solution. *Chem. Phys. Lett.* **1994**, *227*, 19–25.

- (32) Mukamel, S. Photochemistry: Trees to Trap Photons. *Nature* **1997**, *388*, 425–427.
- (33) Kopelman, R.; Shortreed, M.; Shi, Z. Y.; Tan, W.; Xu, Z.; Moore, J. S.; Bar-Haim, A.; Klafter, J. Spectroscopic Evidence for Excitonic Localization in Fractal Antenna Supermolecules. *Phys. Rev. Lett.* **1997**, *78*, 1239–1242.
- (34) Fernandez-Alberti, S.; Roitberg, A. E.; Kleiman, V. D.; Nelson, T.; Tretiak, S. Shishiodoshi Unidirectional Energy Transfer Mechanism in Phenylene Ethynylene Dendrimers. *J. Chem. Phys.* **2012**, *137*, 22A526.
- (35) Fernandez-Alberti, S.; Kleiman, V. D.; Tretiak, S.; Roitberg, A. E. Unidirectional Energy Transfer in Conjugated Molecules: The Crucial Role of High-Frequency C≡C Bonds. *J. Phys. Chem. Lett.* **2010**, *1*, 2699–2704.
- (36) Lira-Cantu, M.; Krebs, F. Hybrid Solar Cells Based on MEH-PPV and Thin Film Semiconductor Oxides (TiO₂, Nb₂O₅, ZnO, CeO₂ and CeO₂/TiO₂): Performance Improvement During Long-Time Irradiation. *Sol. Energy Mater. Sol. Cells* **2006**, *90*, 2076–2086.
- (37) Nelson, T.; Fernandez-Alberti, S.; Roitberg, A. E.; Tretiak, S. Conformational Disorder in Energy Transfer: Beyond Förster Theory. *Phys. Chem. Chem. Phys.* **2013**, *15*, 9245–9256.
- (38) Nelson, T.; Fernandez-Alberti, S.; Roitberg, A. E.; Tretiak, S. Artifacts Due to Trivial Unavoided Crossings in the Modeling of Photoinduced Energy Transfer Dynamics in Extended Conjugated Molecules. *Chem. Phys. Lett.* **2013**, *590*, 208–213.
- (39) Collini, E.; Scholes, G. Coherent Intrachain Energy Migration in a Conjugated Polymer at Room Temperature. *Science* **2009**, *323*, 369–373.
- (40) Tretiak, S.; Zhang, W. M.; Chernyak, V.; Mukamel, S. Excitonic Couplings and Electronic Coherence in Bridged Naphthalene Dimers. *Proc. Natl. Acad. Sci. U.S.A.* **1999**, *96*, 13003–13008.
- (41) Tretiak, S.; Mukamel, S. Density Matrix Analysis and Simulation of Electronic Excitations in Conjugated and Aggregated Molecules. *Chem. Rev.* **2002**, *102*, 3171–3212.
- (42) Dewar, M. J. S.; Zoebisch, E. G.; Healy, E. F.; Stewart, J. J. P. Development and Use of Quantum Mechanical Molecular Models. 76. AM1: A New General Purpose Quantum Mechanical Molecular Model. *J. Am. Chem. Soc.* **1985**, *107*, 3902–3909.
- (43) Dreuw, A.; Head-Gordon, M. Single-Reference ab Initio Methods for the Calculation of Excited States of Large Molecules. *Chem. Rev.* **2005**, *105*, 4009–4037.
- (44) Tretiak, S.; Middleton, C.; Chernyak, V.; Mukamel, S. Bacteriochlorophyll and Carotenoid Excitonic Couplings in the LH2 System of Purple Bacteria. *J. Phys. Chem. B* **2000**, *104*, 9540–9553.
- (45) Tommasini, M.; Chernyak, V.; Mukamel, S. Electronic Density-Matrix Algorithm for Nonadiabatic Couplings in Molecular Dynamics Simulations. *Int. J. Quantum Chem.* **2001**, *85*, 225–238.
- (46) Chernyak, V.; Mukamel, S. Density-Matrix Representation of Nonadiabatic Couplings in Time-Dependent Density Functional (TDDFT) Theories. *J. Chem. Phys.* **2000**, *112*, 3572–3579.
- (47) Tretiak, S.; Chernyak, V. Resonant Nonlinear Polarizabilities in the Time-Dependent Functional Theory. *J. Chem. Phys.* **2003**, *119*, 8809–8823.
- (48) Furche, F.; Ahlrichs, R. Adiabatic Time-Dependent Density Functional Methods for Excited State Properties. *J. Chem. Phys.* **2002**, *117*, 7433–7447.
- (49) Furche, F. On the Density Matrix Based Approach to Time-Dependent Density Functional Response Theory. *J. Chem. Phys.* **2001**, *114*, 5982–5992.
- (50) Granucci, G.; Persico, M.; Toniolo, A. Direct Semiclassical Simulation of Photochemical Processes with Semiempirical Wave Functions. *J. Chem. Phys.* **2001**, *114*, 10608–10615.
- (51) Mukamel, S.; Tretiak, S.; Wagersreiter, T.; Chernyak, V. Electronic Coherence and Collective Optical Excitations of Conjugated Molecules. *Science* **1997**, *277*, 781–787.
- (52) Robb, M. A.; Garavelli, M.; Olivucci, M.; Bernardi, F. *Reviews in Computational Chemistry*; Wiley-VCH: New York, 2000; Vol. 15.
- (53) Domcke, W.; Yarkony, D. R.; Koppel, H. *Conical Intersections: Electronic, Structure, Dynamics and Spectroscopy*; World Scientific: Singapore, 2004.
- (54) Yarkony, D. R. Diabolical Conical Intersections. *Rev. Mod. Phys.* **1996**, *68*, 985–1013.
- (55) Yarkony, D. R. Conical Intersections: The New Conventional Wisdom. *J. Phys. Chem. A* **2001**, *105*, 6277–6293.
- (56) Plasser, F.; Granucci, G.; Pittner, J.; Barbatti, M.; Persico, M.; Lischka, H. Surface Hopping Dynamics Using a Locally Diabatic Formalism: Charge Transfer in the Ethylene Dimer Cation and Excited State Dynamics in the 2-Pyridone Dimer. *J. Chem. Phys.* **2012**, *137*, 22A514.
- (57) Kalstein, A.; Fernandez-Alberti, S.; Bastida, A.; Soler, M. A.; Farag, M. H.; Zúñiga, J.; Requena, A. Vibrational Dynamics of Polyatomic Molecules in Solution: Assignment, Time Evolution and Mixing of Instantaneous Normal Modes. *Theor. Chem. Acc.* **2010**, *128*, 769–782.
- (58) Duschinsky, F. On the Interpretation of Electronic Spectra of Polyatomic Molecules. *Acta Physicochim.* **1937**, *7*, 551–556.
- (59) Billing, G. D. Classical Path Method in Inelastic and Reactive Scattering. *Int. Rev. Phys. Chem.* **1994**, *13*, 309–335.